Physics-based Creep Simulations of Thick Section Welds in High Temperature and Pressure Applications

Thomas M. Lillo, PI, Testing & Validation
Wen Jiang, Co-PI, Modeling and Simulation
Idaho National Laboratory
P.O. Box 1625
Idaho Falls, ID 83415
Thomas.Lillo@INL.gov

2018 NETL Annual Review Meeting for Crosscutting Research, April 10-12, 2017, Pittsburgh, PA

Date: April 11, 2018

DOE Award Number: FEAA90

Period of Performance: 07/2015-09/2018

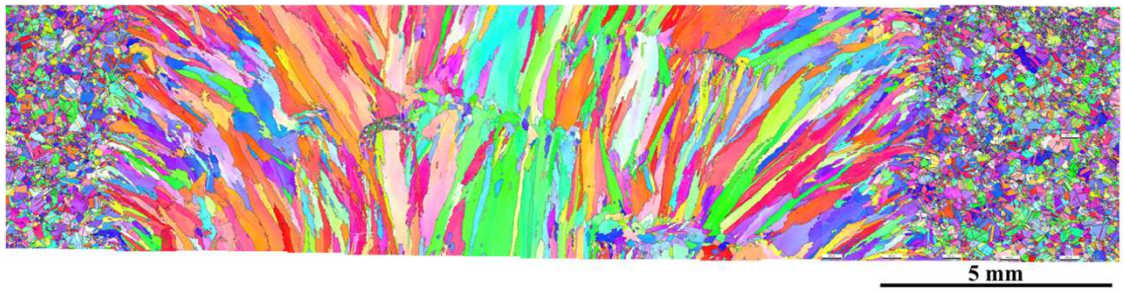

Project Goals and Objectives

Goal: Develop modeling and simulation capabilities to describe/predict the creep behavior of thick section welds in Alloy 740H (a γ'– strengthened, Ni-based alloy for a-USC applications)

- Computational modeling development of physical processes involved in the creep of welds in Alloy 740H across length scales:
  - Diffusion
  - Dislocation motion and deformation
  - Microstructural evolution
  - Uniaxial cross-weld creep specimen behavior
- Develop/modify individual computational "modules" within the MOOSE computational architecture to describe each physical process:
  - Dislocation glide/climb
  - Dislocation/γ' interaction
    - γ' shearing
    - Dislocation climb over γ' particles
    - Dislocation looping of γ'
  - Incorporate experimental microstructures and their evolution

Project Goals and Objectives – cont.

- Experimental Testing and Validation
  - Cross-weld creep testing
  - γ' aging for particle size evolution
    - Weld
    - Base metal
  - Threshold stress as a function of γ' evolution and temperature
  - Microstructural characterization for the generation of synthetic microstructures
    - Weld
    - Base metal

Presentation Outline

- Modeling and simulation approach
  - Overview of the MOOSE architecture
  - Power law creep – incorporation of dislocation climb
  - Dislocation interaction with γ' particles
    - Particle shearing
    - Dislocation climb bypass
    - Orowan looping
- Experimental Studies supporting modeling
  - Creep tests of weld
  - Microstructural characterization and synthetic microstructure generation
  - γ' evolution
  - Threshold stress determination as a function of temperature and γ' radius
  - Weld microstructure refinement through hybrid laser arc welding

Modeling and Simulation Approach – MOOSE Architecture

MOOSE

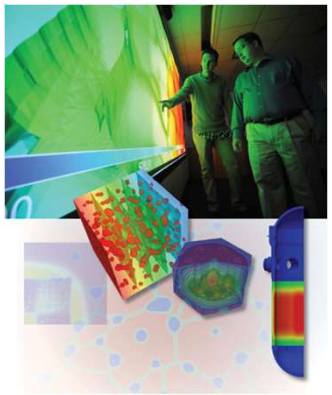

R&D 100 2014 Winner

- MOOSE is a finite element, multiphysics framework that simplifies the development of advanced numerical applications.
- It provides a high-level interface to sophisticated nonlinear solvers and massively parallel computational capability.
- Open Source, available at http://mooseframework.org

Framework

All of the code that forms the basis of the MOOSE framework

Modules

Phase Field

- Cahn-Hilliard equation
- Allen-Cahn equations
- Free energy based development

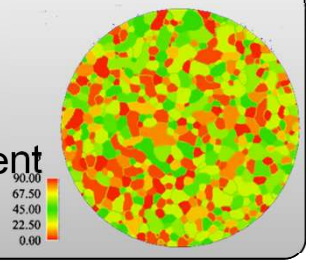

Tensor Mechanics

- Linear elasticity
- Eigenstrains
- J2 Plasticity
- Crystal plasticity

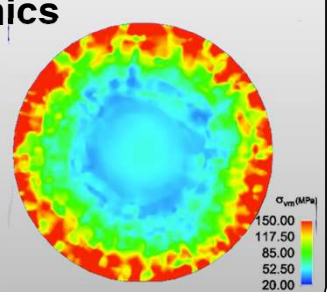

Modeling approach

- Polycrystalline length scale – region consisting of base metal, HAZ and fusion region

  - FIB, EBSD, SEM – Grain size, orientation, misorientation distribution
  - Reconstructed or synthetic microstructure satisfying the statistics

Diffusional creep:
Lattice site generation/annihilation model

Dislocation creep:
Dislocation density based model considering APB shearing, Orowan loop and climb

Effect of γ' shape, size, volume fraction on APB shear - Homogenized model from micromechanics simulation

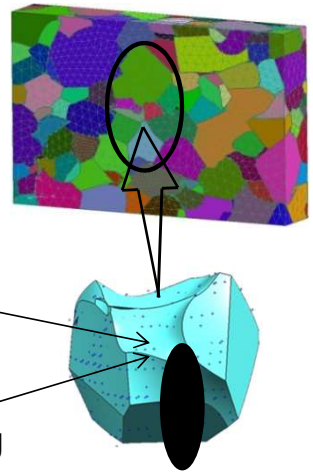

Representative Volume of polycrystalline microstructure

Evolution of γ' precipitate

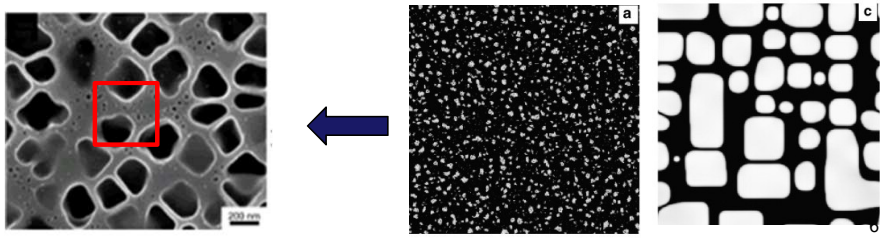

Dislocation density based Crystal plasticity model

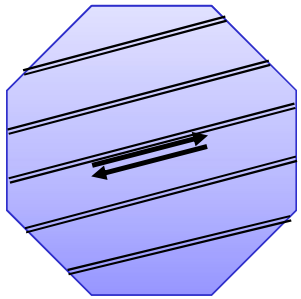

dislocation slip along slip planes

$$\boldsymbol{F} = \boldsymbol{F}^{\boldsymbol{e}}\boldsymbol{F}^{\boldsymbol{p}}$$ Elastic and plastic deformation gradient

Plastic velocity gradient in the intermediate configuration

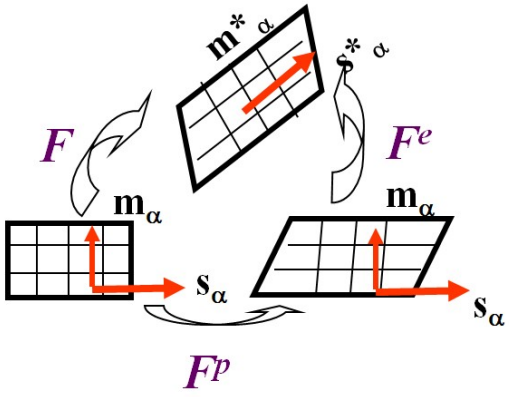

$$\dot{\boldsymbol{F}}^{\boldsymbol{p}}\boldsymbol{F}^{\boldsymbol{p-1}} = \sum_{\alpha=1}^{N_S} \dot{\gamma}^{a}_{glide}\boldsymbol{S}_{\boldsymbol{0}}^{\boldsymbol{\alpha}} + \sum_{\alpha=1}^{N_C} \dot{\gamma}^{a}_{climb}\boldsymbol{N}_{\boldsymbol{0}}^{\boldsymbol{\alpha}}$$

$$\boldsymbol{S}_{\boldsymbol{0}}^{\boldsymbol{\alpha}} = \boldsymbol{m}_{\boldsymbol{0}}^{\boldsymbol{\alpha}} \otimes \boldsymbol{n}_{\boldsymbol{0}}^{\boldsymbol{\alpha}}$$ Glide direction

$$\boldsymbol{N}_{\boldsymbol{0}}^{\boldsymbol{\alpha}} = \boldsymbol{m}_{\boldsymbol{0}}^{\boldsymbol{\alpha}} \otimes \boldsymbol{m}_{\boldsymbol{0}}^{\boldsymbol{\alpha}}$$ Climb direction

s - Slip direction *m* - normal in reference configuration

Glide model

Glide rate : $\dot{\gamma}^a_{glide} = (1-\phi_p)\rho^\alpha_M b v^\alpha_g$

- ϕ_p : precipitate volume fraction. The glide is limited to the matrix channels
- ρ_M : mobile dislocation density

Activation enthalpy driven flow rule

- Glide Velocity $v^\alpha_g = \begin{cases} l\nu \exp\left(-\frac{\Delta F_g}{KT}\left(1-\left(\frac{|\tau^\alpha_g|-s^\alpha_a}{s^\alpha_t}\right)^p\right)^q\right)\mathrm{sgn}(\tau^\alpha_g); |\tau^\alpha_g| > s^\alpha_a \\ 0; |\tau^\alpha_g| \leq s^\alpha_a \end{cases}$
- Resolved shear stress $\tau^\alpha_g = \boldsymbol{T} : \boldsymbol{m^\alpha_0} \otimes \boldsymbol{n^\alpha_0}$
- Athermal resistance $s^\alpha_a = \tau^\alpha_{disloc-disloc} = Gb\sqrt{\sum_{\zeta=1}^{N_S} q_\rho A^{\alpha\zeta}\rho^\zeta}$

Vacancy diffusion-induced climb model

At elevated temperatures, **bulk diffusion of vacancies** usually **dominates** the dislocation climb model. The rate of vacancy absorption is limited by the rate at which vacancies are absorbed at jogs along dislocation line.

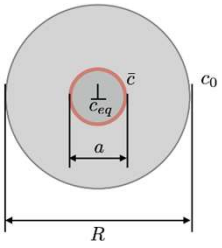

Climb component of Peach-Koehler force $\tau_c^\alpha = -b\boldsymbol{T} : \boldsymbol{m_0^\alpha} \otimes \boldsymbol{m_0^\alpha}$

Climb velocity $v_c^\alpha = -\dfrac{2\pi D}{b\log(r_\infty^\alpha / r_c)}\left(c_{eq}^\alpha - c_0\right)$ $\quad c_{eq}^\alpha = c_0 \exp\left(-\dfrac{\tau_c^\alpha V_m}{bRT}\right)$

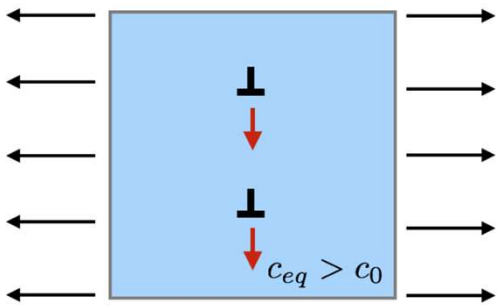

Tension: **emit** vacancy, climb **down**

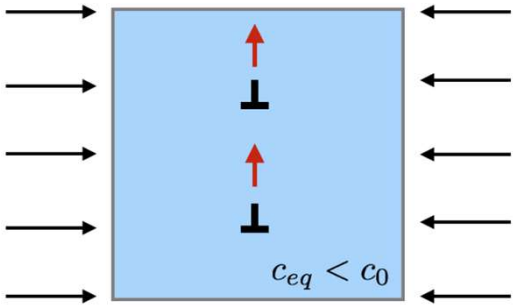

Compression: **absorb** vacancy, climb **up**

The mobile dislocation in contact with precipitates is $\phi_p \rho_M^\alpha$

Climb rate: $\dot{\gamma}_{climb}^a = -\phi_p \rho_M^\alpha b v_c^\alpha$

Orowan Looping

Orowan looping Orowan looping occurs when the stress required for a dislocation to bow between precipitates is less than the stress required for the dislocation to penetrate precipitates

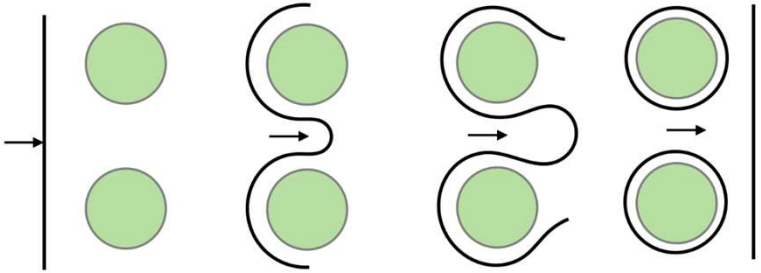

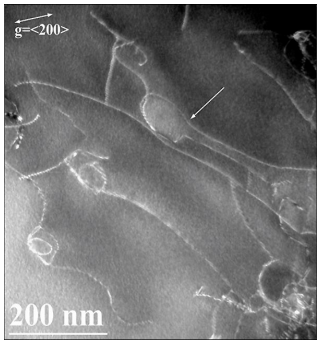

γ' particle bypass by dislocation looping (Alloy 617)

Stress above which looping will occur was determined by

$$\tau_{looping} = \frac{Gb}{L_s}$$

Spacing between precipitates $L_s = \sqrt{\frac{8}{3\pi\phi_p}} r_p - r_p$

The athermal resistance is increased by the Orowan looping :

$$s_a^{\alpha} = \sqrt{{\tau_{disloc-disloc}^{\alpha}}^2 + \tau_{looping}^2}$$

Dislocation density evolution

Dislocation density evolution $\dot{\rho^{\alpha}} = \dot{\rho_M^{\alpha}} + \dot{\rho_I^{\alpha}}$

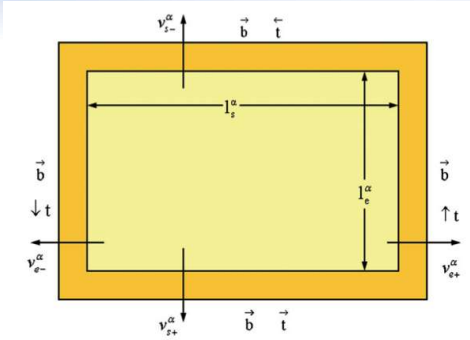

Evolution of mobile dislocation density

Dislocation multiplication from Frank-Read source and loop expansion

Annihilation of dislocations of opposite signs

$$\dot{\rho}_M^{\alpha} = \frac{k_{mul}}{b}\sqrt{\sum_{\zeta}\rho_M^{\zeta}}|\dot{\gamma}_{glide}^{a}| - \frac{R_c}{b/2}\rho_M^{\alpha}\left(|\dot{\gamma}_{glide}^{a}| + |\dot{\gamma}_{climb}^{a}|\right)$$

$$-\frac{\beta_{\rho}\sqrt{\rho^{\alpha}}}{b}\left(|\dot{\gamma}_{glide}^{a}| + |\dot{\gamma}_{climb}^{a}|\right) - \alpha_D\varphi\frac{\sqrt{\phi_p}}{r}|\dot{\gamma}_{glide}^{a}| + \frac{|\dot{\gamma}_{climb}^{a}|}{br}$$

Dislocation trapping

Storage of Orowan loops

Mobilization of Dislocations

Evolution of immobile dislocation density

$$\dot{\rho}_I^{\alpha} = \frac{\beta_{\rho}\sqrt{\rho^{\alpha}}}{b}\left(|\dot{\gamma}_{glide}^{a}| + |\dot{\gamma}_{climb}^{a}|\right) + \alpha_D\varphi\frac{\sqrt{\phi_p}}{r_p}|\dot{\gamma}_{glide}^{a}| - \frac{|\dot{\gamma}_{climb}^{a}|}{br_p}$$

Dislocation trapping

Storage of Orowan loops

Mobilization of Dislocations

Alloy 617 simulation results

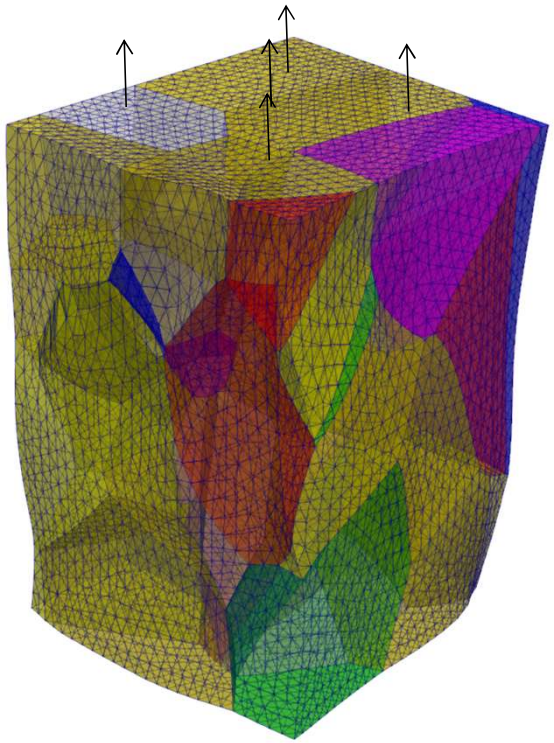

50 grains and 150k elements

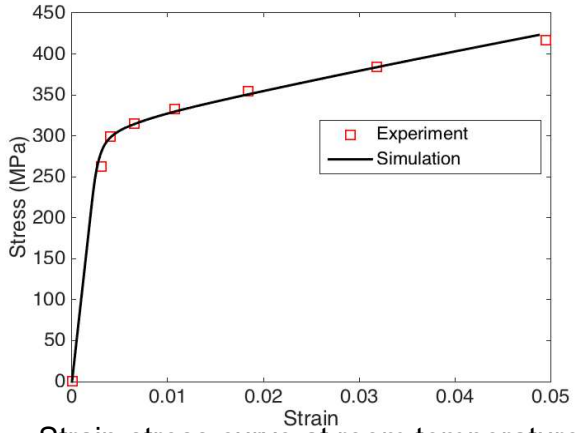

Strain-stress curve at room temperature for constant strain rate loading.

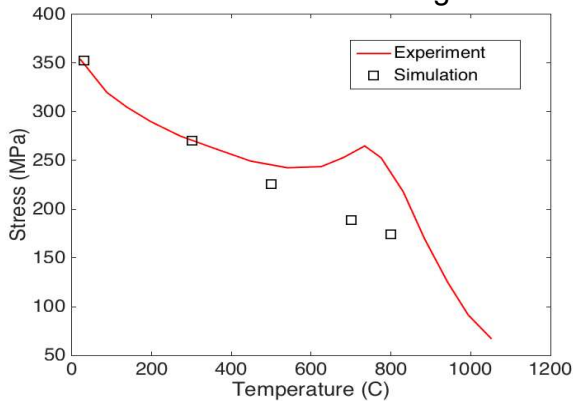

Yield strength with temperature.

Alloy 617 simulation results

Glide (not incorporated Orowan looping) and climb calibration results

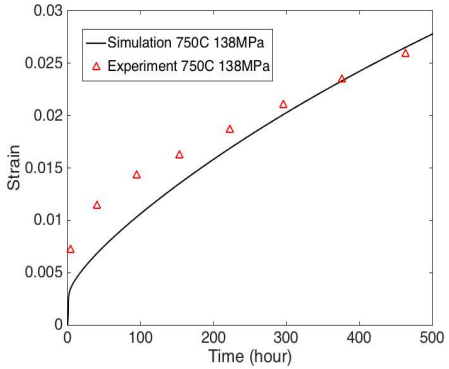

750°C and 138 MPa

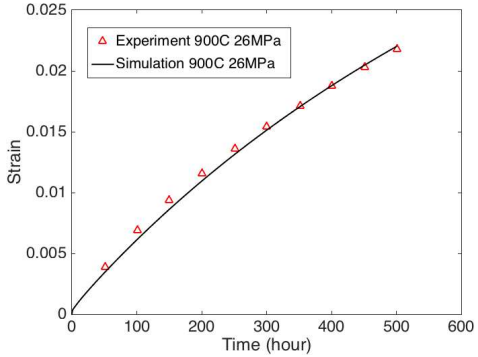

900°C and 26 MPa

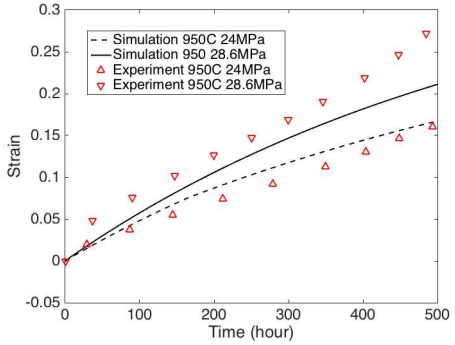

950°C and 24 and 28.6 MPa

Experimental Studies – Creep Testing

- Creep tests will be carried out at or below the aging temperature
  - Short term creep tests – support modeling and validation of modules
    - All-weld metal gage section – longitudinal orientation in weld
    - Transverse weld gage section
  - Long term creep test – validate simulation

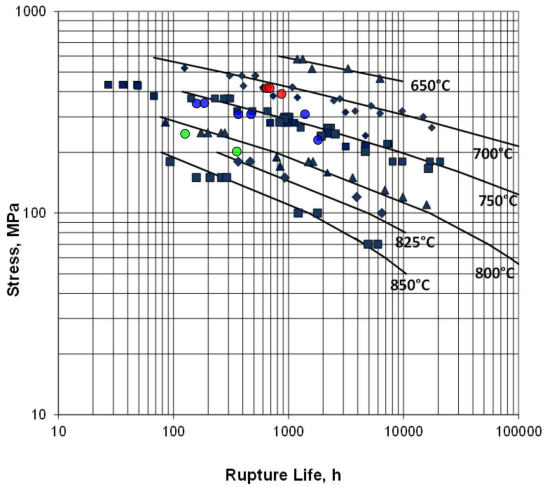

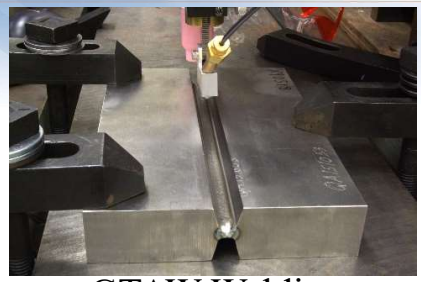

GTAW Welding

PWHT

Short-term Creep Test Matrix

Specimen ID	Test Temperature, °C	Test type	Initial Stress, MPa	Orientation	Actual Rupture, hrs	Minimum Creep Rate, %/second
740-Q1-1	700	Creep rupture	413	Cross weld	639	3.2E-7
740-Q1-8	700	Creep rupture	413	Cross weld	670.8	3.2E-7
740-Q1-6	700	Creep rupture	395	Cross weld	879	2.1E-7
740-Q1-3	750	Creep rupture	350	Cross weld	184	14.6E-7
740-Q2-1	750	Creep Rupture	350	Cross weld	162.1	8.4E-7
740-Q1-5	750	Creep rupture	305	Cross weld	450	6.0E-07
740-Q2-2	750	Creep Rupture	305	Cross weld	354.3	3.2E-7
740-Q1-10	750	Creep rupture	230	Cross weld	1749.4	1.5E-7
740-Q1-4	800	Creep rupture	240	Cross weld	123.6	23.1E-7
740-Q1-2	800	Creep rupture	200	Cross weld	326.8	8.6E-7
	800	Creep rupture	138	Cross weld		
	700	Creep rupture	413	All weld metal		
740-AWM-01	750	Creep rupture	305	All weld metal	1297.5	1.1E-7
	800	Creep rupture	200	All weld metal		

Long–term Creep Validation Matrix

Test Temperature, °C	Specimen ID	Initial Stress, MPa	Orientation	Expected Rupture Life, hrs	Actual Rupture Life, hrs	Minimum Creep Rate, %/second	Ductility, %
700		214	Cross weld	9700			
750	740-Q1-9	141	Cross weld	9700	11011	0.35E-7	5.3
800	740-Q1-7	83	Cross weld	9700	4680	1.1E-7	5.9

Synthetic Microstructures

- 3D volume needed for simulations
- EBSD on three orthogonal surfaces
- Reconstructed in Dream 3D
  - Morphology
  - Orientation statistics

Issues

- Scale of weld requires multiple, large data files for base and weld metal
- Increase EBSD scan step size but lose resolution – serial sectioning
- "Mesh" directly in Dream 3D using voxel representation of the grains

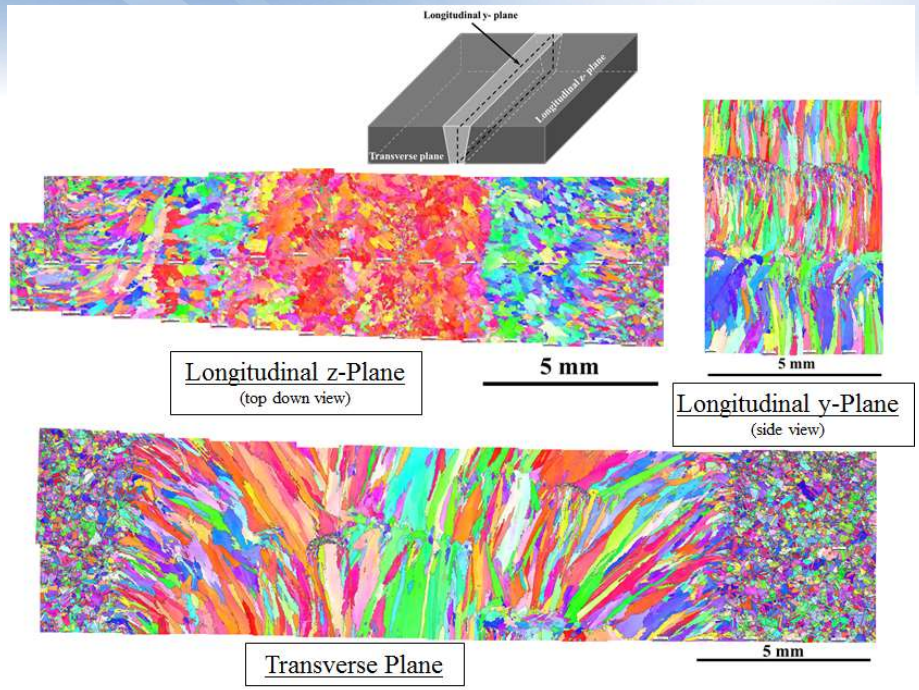

EBSD Data

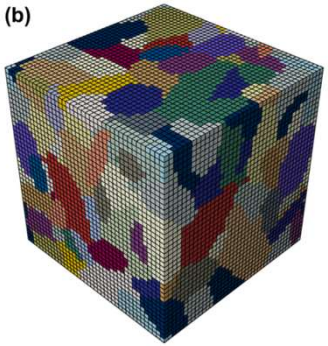

Dream 3D "mesh" based on voxels

γ' Aging in the Weld

Concerns:

- γ' growth during creep
- Weld metal (compositional effects?)

Goal:

- Determine growth rate constant as a function of temperature, *k(T),* for modeling effort:

$$r^3 - r_o^3 = k(T)t$$

Experimental:

- Temperatures: 700, 750, 800°C
- Aging times up to 10,000 hrs
- TEM with image analysis

Results:

- γ' growth behavior at 750°C follows that of Alloy 617
- More statistical variation of γ' size in weld

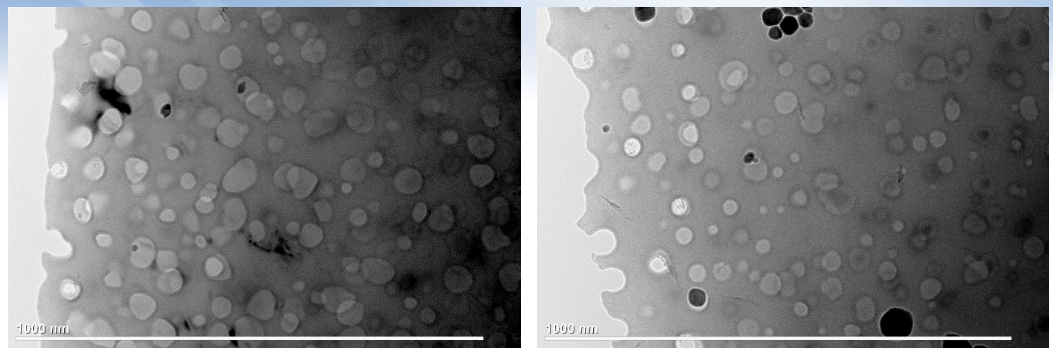

γ' fraction variation in weld (Aged - 750°C, 400 hrs)

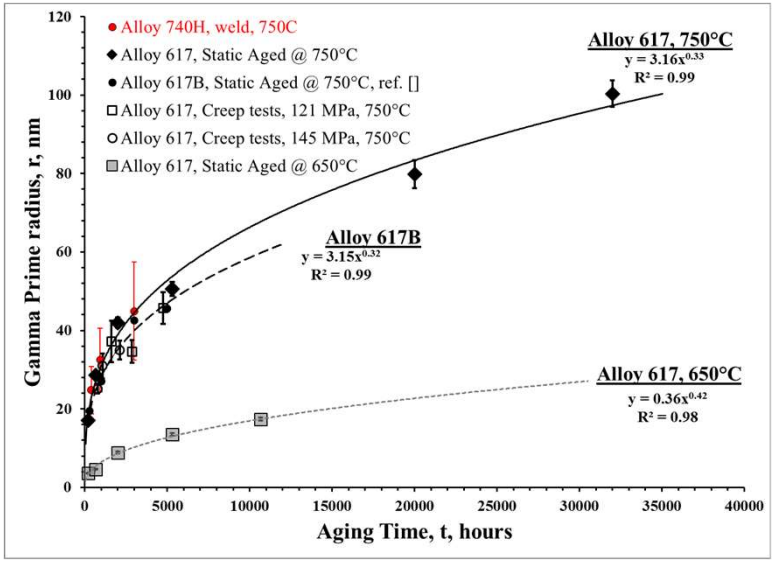

Threshold Stress Determination from Stress Drop Creep Tests

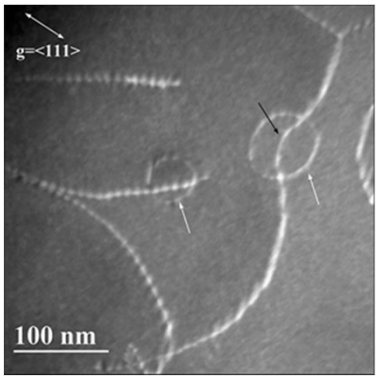

γ' particle bypass by dislocation climb

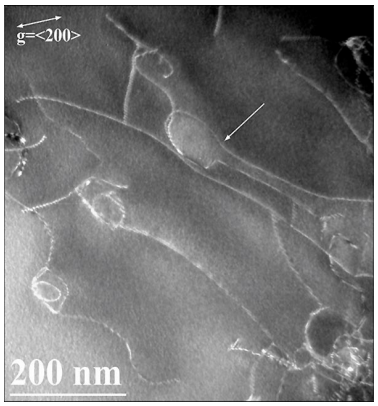

γ' particle bypass by dislocation looping

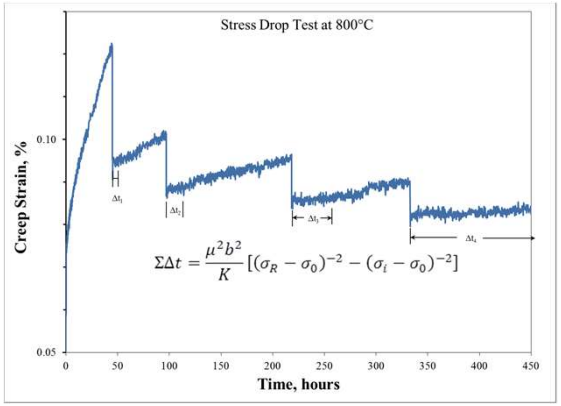

Results of Stress Drop Testing			
Aging Condition	**Aging description***	**Test Temperature**	**Threshold stress, MPa**
0	PWHT	700	
0	PWHT	750	136
0	PWHT	800	94
1	PWHT+4000 hrs	700	283
1	PWHT+4000 hrs	750	98
1	PWHT+4000 hrs	800	49
2	PWHT+8000 hrs	700	
2	PWHT+8000 hrs	750	98
2	PWHT+8000 hrs	800	
* Aging performed at 750°C			

TML1

Idaho National Laboratory

Weld Microstructure Refinement with Hybrid Laser Arc Welding

Justification

- GTAW welds show low ductility (<10%)
- Weld grain size very large
- Hybrid Laser Arc Welds:
  - Many Economical Advantages
  - Low heat input
  - Refined microstructure
  - Increased creep ductility?

Preliminary Results

- Defect in the laser portion of welds
- Some cracking in arc portion of welds – more evident at higher speeds

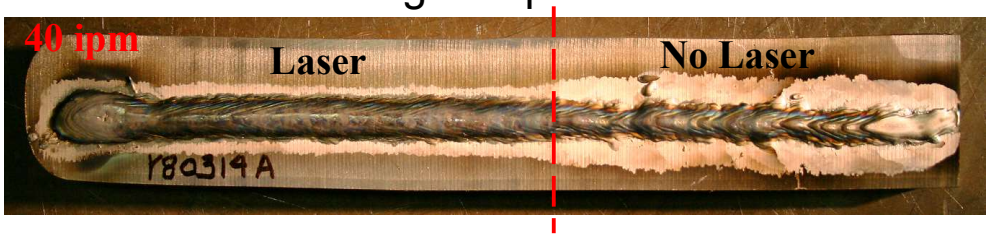

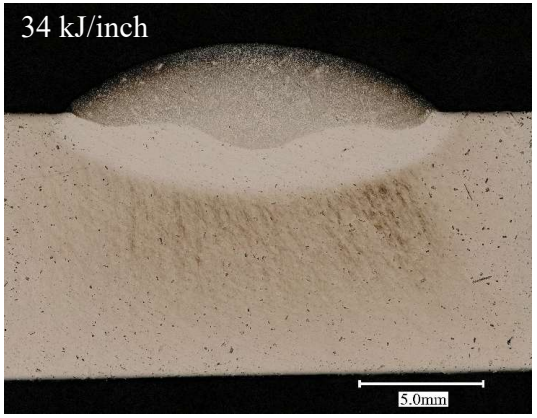

No Laser - 10 ipm

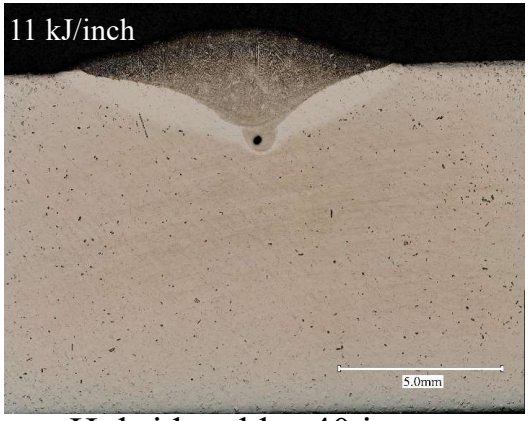

Hybrid weld - 40 ipm

Weld parameters
- Arc power - kW
- Laser power – 2 kW

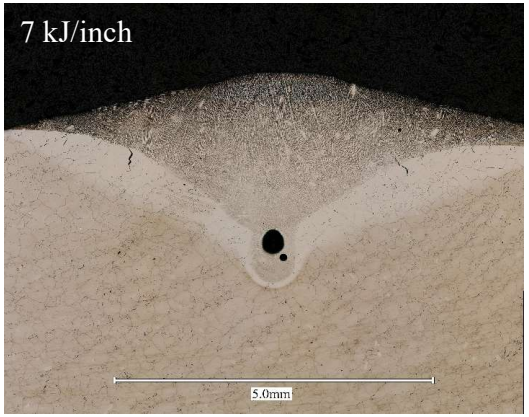

Hybrid weld - 65 ipm

Slide 18

TML1 Thomas M. Lillo, 4/4/2018

Questions

Contact Information

- Thomas Lillo:
  - Thomas.Lillo@inl.gov
  - (208)526-9746
- Wen Jiang:
  - Wen.Jiang@inl.gov
  - (208)526-1586